Research Square

Preprints are preliminary reports that have not undergone peer review.
They should not be considered conclusive, used to inform clinical practice,
or referenced by the media as validated information.

An open-source, high-torque, and portable hip exoskeleton for physically demanding locomotion

Patrick Slade

slade@seas.harvard.edu

Harvard University https://orcid.org/0000-0001-9302-3911

Jae-Ryeong Choi

Harvard University

Yinkai Dong

Harvard University https://orcid.org/0000-0002-4542-7177

Catherine Rohner

Harvard University https://orcid.org/0009-0005-3610-1449

Article

Keywords:

Posted Date: November 18th, 2026

DOI: https://doi.org/10.21203/rs.3.rs-9379840/v1

License: This work is licensed under a Creative Commons Attribution 4.0 International License.
Read Full License

Additional Declarations: There is **NO** Competing Interest.

Title: An open-source, high-torque, and portable hip exoskeleton for physically demanding locomotion

Authors: Jae-Ryeong Choi[1], Yinkai Dong[1], Catherine Rohner[1,2], and Patrick Slade[1,3*]

Affiliations:
[1]John A. Paulson School of Engineering and Applied Sciences, Harvard University, Boston, MA, USA.
[2]Department of Health Sciences and Technology, ETH Zurich, Zurich, Switzerland,
[3]Kempner Institute for the Study of Natural and Artificial Intelligence, Harvard University, Boston, MA, USA.
*Corresponding author, Email: slade@seas.harvard.edu

Abstract: Physically demanding jobs such as emergency services, construction, and military operations often require people to overcome challenging inclined terrain that increases their risk of injury and fatigue. Although exoskeletons are a promising tool for assisting human locomotion, few devices have demonstrated substantial reductions in energy expenditure during physically demanding activities. Here, we present the Open-source, High-torque, and Portable (OpenHi-P) hip exoskeleton that reduces the absolute metabolic cost of walking, compared to not wearing the exoskeleton, by approximately twice that of any portable lower-limb exoskeleton and three times that of any portable hip exoskeleton in studies of healthy adults that met our inclusion criteria. Healthy young adults completed a multi-day experiment where human-in-the-loop optimization identified personalized exoskeleton assistance for each user during treadmill walking at 1 m/s and a 10° incline. Personalized assistance reduced the metabolic cost of incline walking by 2.1 W/kg (22%) compared to not wearing the exoskeleton (n = 8). In a preliminary experiment that emulated a physically demanding firefighter training protocol, personalized assistance also reduced the cost of transport by 2.6 J/(m·kg) (20%) compared to not wearing the exoskeleton (n = 4) during repeated bouts of inclined and loaded walking. In a preliminary outdoor experiment on uneven and inclined terrain, personalized assistance reduced the cost of transport by 1.6 J/(m·kg) (20%) and increased speed by 9% compared to not wearing the exoskeleton (n = 4). This open-source, portable hip exoskeleton can substantially reduce the energetic cost of physically demanding tasks and accelerate exoskeleton development.

Introduction

Many jobs require people to perform physically demanding tasks on challenging inclined terrain that can cause fatigue and increase the risk of injury. Firefighters frequently encounter steep inclines while carrying personal protective equipment, contributing to overexertion or strain which are the leading causes of firefighter injuries[1]. Similar demands are common in military operations, where uneven and inclined terrain is a recognized risk factor for lower-extremity musculoskeletal injuries[2]. These physically demanding tasks are associated with high biomechanical and metabolic demands that increase lower-limb joint moment and power requirements[3], ultimately contributing to muscular fatigue[4]. Repeated exposure to these physically demanding tasks can degrade locomotor stability[5], increasing the likelihood of health risks such

as slips, trips, and falls[6]. There is a need to support people who perform physically demanding tasks to reduce health risks.

Portable exoskeletons show promise for assisting demanding tasks like incline walking, but currently only provide moderate reductions in metabolic cost because it is challenging to determine the device, assistance, and protocol requirements for best-case benefits. Portable exoskeletons often assist a single joint to minimize device mass and complexity, with previous devices providing an average positive mechanical power from 0.15 to 0.37 W/kg[7–13] and achieving a metabolic reduction from 0.12 to 1.08 W/kg[14–19] compared to not wearing the exoskeleton. However, there are many factors that contribute to an exoskeleton's potential metabolic reductions, including: the maximum power or torque the device can provide[20,21], the device weight[22], personalization of assistance to each user[23], and sufficient training time to allow users to benefit most from the device[24]. Lab-based exoskeleton emulators aim to disentangle these interrelated challenges by providing a device that can explore a wide range of assistance profiles with powerful offboard motors[25–28]. Emulator experiments often perform multi-day assistance optimization protocols that personalize assistance[23] and train users[24] to maximize the benefit of assistance.

A portable hip exoskeleton with an emulator-informed design and an experimental protocol that personalizes assistance and trains users may be able to achieve a large metabolic reduction during real-world incline walking. Prior portable exoskeletons that were designed to provide the idealized assistance from lab-based emulator studies achieved best-case metabolic reductions for walking[17] and running[29,30]. For incline walking, a lab-based emulator provided hip (1.2 W/kg), knee (0.6 W/kg), and ankle (0.3 W/kg) assistance at a 10° incline[25], with the hip assistance alone providing 3 to 8 times the mechanical power of portable exoskeletons and achieving larger metabolic reductions. The hip, knee, and ankle joint contributions to the total joint power demands during incline walking are 52%, 19%, and 28%, respectively[31]. Based on these emulator and biomechanical studies, the hip may be the most promising single joint to assist during incline walking.

We developed the Open-source, High-torque, and Portable (OpenHi-P) hip exoskeleton and performed a multi-day experimental protocol to dramatically reduce the metabolic cost of incline walking compared to not wearing the exoskeleton. The exoskeleton hardware design was adapted from the lab-based emulator study of incline walking[25] to provide similarly high assistance power, while maintaining portability with a similar mass to single-joint portable exoskeletons. We conducted a multi-day human-in-the-loop optimization to identify participant-specific assistance profiles and train users with the exoskeleton. The personalized exoskeleton assistance was compared to not wearing the exoskeleton during incline walking on a treadmill and on real-world, inclined terrain. This work demonstrates effective exoskeleton assistance for physically demanding activities and design principles for high-torque, portable exoskeletons.

Results

Participants completed a human-in-the-loop optimization protocol to systematically tune exoskeleton assistance and then evaluate validation conditions with and without the exoskeleton. Eight participants (4 men and 4 women; age, 26.8±3.3 yr; body mass, 65.1±9.8 kg; height, 1.70±0.07 m; Supplementary Table 1) were recruited for a multi-day experimental protocol. Participants completed eight generations of optimization to tune six hip exoskeleton torque

parameters (Fig. 1a). Each generation consisted of nine assistance conditions, with respirometry data from each 2-min condition estimating the metabolic rate for one set of assistance parameters by fitting a first-order exponential model[28]. After completing all generations of optimization, participants completed three validation conditions (Fig. 1b): not wearing the exoskeleton (no exo), wearing the exoskeleton turned off (exo off), and wearing the exoskeleton while receiving personalized assistance (personalized). Validation conditions lasted 5 minutes and were conducted in a randomized, double-reversal order (Supplementary Table 2).

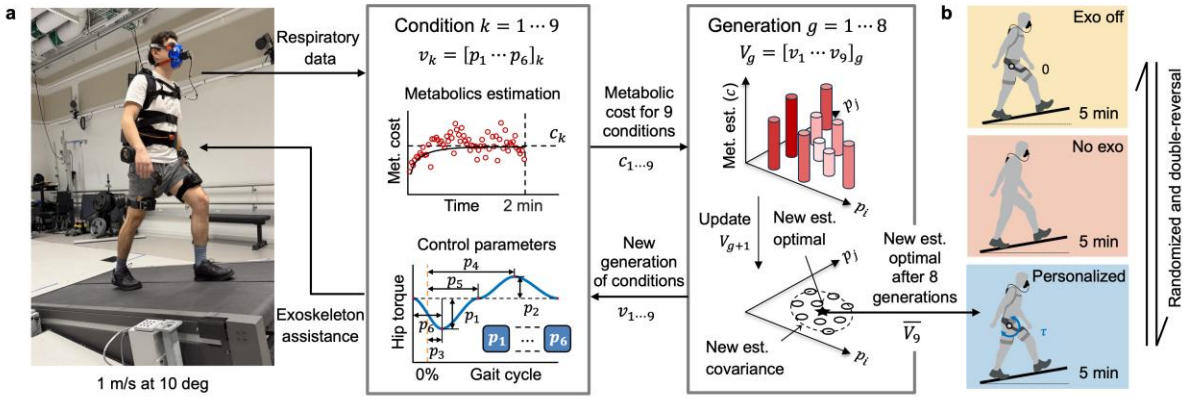


Fig. 1 | Overview of experimental protocol. (a) Human-in-the-loop optimization during treadmill incline walking (10° at 1 m/s). Participants walked while respiratory data estimated metabolic cost. Six control parameters defined the hip assistance profile applied to the user. Participants completed assistance conditions that estimated the metabolic cost of walking with one set of assistance parameters. The optimization consisted of eight generations, with each generation containing nine conditions. **(b)** Participants completed three validation conditions (exo off, no exo, and personalized assistance).

Personalized assistance significantly reduced metabolic cost compared to the no exo condition, providing metabolic benefits approximately twice the largest reduction previously reported for a portable lower-limb exoskeleton in healthy adults[7–19] (Supplementary Table 3). Personalized assistance significantly reduced the metabolic cost of incline walking by 2.1 W/kg (22%; $t(7) = 8.36$, $P < 0.001$, 95% CI [1.48, 2.65], $d_z = 2.96$; Supplementary Table 4) compared to the no exo condition (Fig. 2a). This reduction is 1.9 times the previous best for a portable lower-limb exoskeleton (1.08 W/kg, ankle) and 3.0 times the previous best for a portable hip exoskeleton (0.69 W/kg), using the inclusion criteria defined in the Methods (Fig. 2b). The values compiled for this comparison are given in Supplementary Table 3. The exoskeleton generated an average positive mechanical power of 1.0 ± 0.2 W/kg over the gait cycle, summed over both legs, 2.7 to 6.6 times that of prior portable exoskeletons (Fig. 2c).

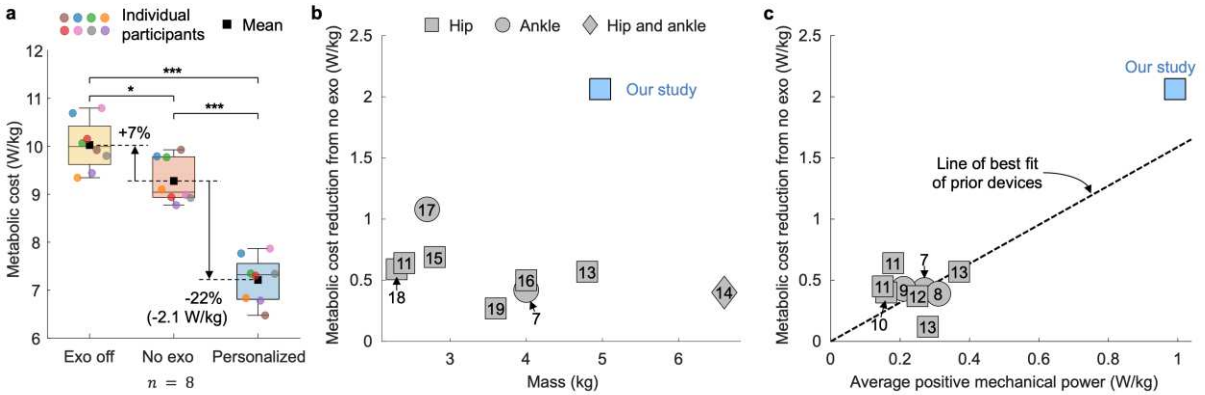


Fig. 2 | Metabolic cost reduction of the OpenHi-P exoskeleton compared with prior portable exoskeletons. (a) Metabolic cost across validation conditions (repeated-measures ANOVA with post hoc paired comparisons, $n = 8$, Bonferroni corrected, *$P < 0.05$, ***$P < 0.001$). Boxes extend from the lower to upper quartiles, the center line indicates the median, and the whiskers extend from the minimum to the maximum data point. **(b)** Absolute metabolic cost reduction relative to no exo compared against device mass. The number on each symbol is the reference number in this paper that corresponds to each prior study. **(c)** Absolute metabolic reduction relative to no exo compared against exoskeleton-side average positive mechanical power of both legs.

We developed a high-torque, portable hip exoskeleton that consists of rigid and textile components, informed by prior lab-based exoskeleton emulator experiments[26]. The exoskeleton emulator provided high torques at the hip while maintaining user comfort by distributing reaction forces over a large interface area and using the longest possible moment arms along the body segments. The OpenHi-P exoskeleton incorporated these same design principles by using rigid elements to construct the primary load-bearing structure from lightweight carbon-fiber and aluminum components, and relying on inextensible textile interfaces elsewhere to reduce mass (Fig. 3a, b). The applied hip torque was directly measured with a load cell to perform closed-loop torque control and track the desired torque profile. Torque tracking performance, quantified as the root-mean-squared error (RMSE) between desired and measured torque, was 1.93 Nm for a representative participant with a peak torque of 42 Nm during incline walking (Fig. 3c), and below 2 Nm across participants (Fig. 3d). Supplementary Movie 1 shows the desired and measured torque during treadmill walking at a 10° incline and 1 m/s with about 40 Nm of extension torque.

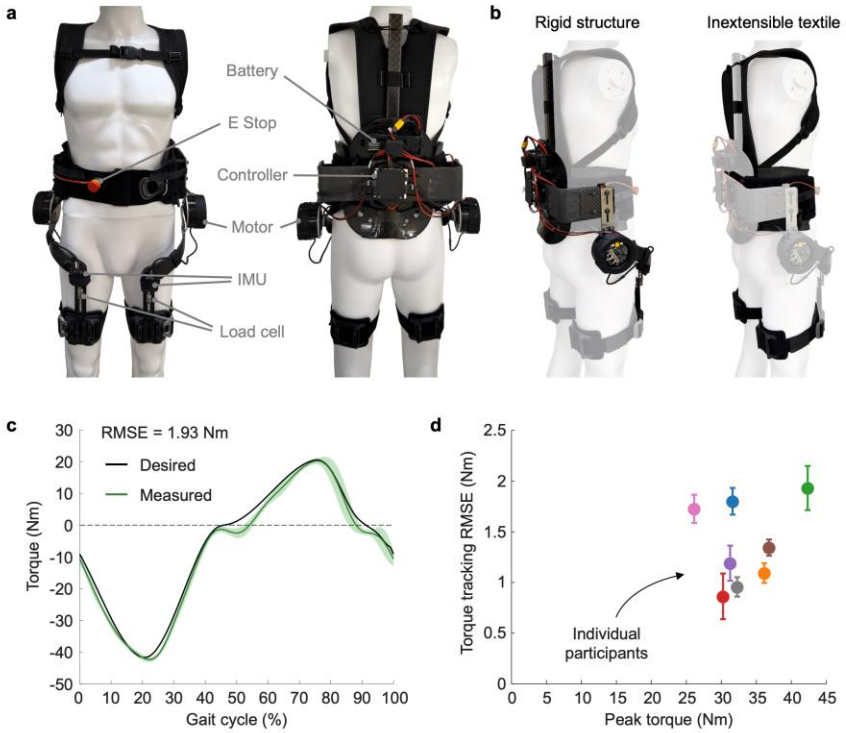


Fig. 3 | The OpenHi-P exoskeleton hardware and torque tracking performance. (a) Front and back views of the hip exoskeleton worn on a mannequin, highlighting mechatronics components. **(b)** Side view of the hip exoskeleton, outlining the rigid, load-bearing structure and the inextensible soft textile interface used to transmit forces to the person. **(c)** Torque tracking performance showing desired and measured hip torque profiles over the gait cycle for a representative participant. **(d)** Torque tracking root-mean-squared error (RMSE) versus measured peak torque for each participant. Points show the RMSE between the mean desired and measured torque profiles, and error bars indicate the within-participant standard deviation of the RMSE.

Analysis of the human-in-the-loop optimization experiment characterized the personalized torque parameters, changes in metabolic cost, and mechanical power generated by the exoskeleton. The optimization systematically tuned six parameters that defined the magnitude and timing of the hip exoskeleton extension and flexion torque profile across the gait cycle (Fig. 4a). The results from a previous lab-based exoskeleton emulator optimization study[25] and pilot experiments informed the selection of parameter boundaries that were safe to evaluate and provided the largest range of potential parameters to search during optimization (Fig. 4b; Supplementary Table 5). The metabolic cost of walking decreased progressively across generations of human-in-the-loop optimization while participants were also being trained with the device (Fig. 4c). The personalized parameters were selected as the mean of the nine parameter sets proposed after completing the eight generations of optimization and were unique for each individual (Fig. 4d). Participants had personalized torque profiles, such as peak extension torques ranging from 26 to 43 Nm (Fig. 4e). The corresponding mechanical power profiles across the gait cycle showed large positive power during the stance phase, consistent with the high extension torques (Fig. 4f).

Personalized assistance reduced muscle activation for several lower-limb muscles compared to the no exo condition. Muscle activation reductions were most pronounced during the stance phase (Fig. 5a). Personalized assistance significantly reduced activation in the primary hip extensor muscles compared to the no exo condition (Fig. 5b), including the gluteus maximus (25%; $t(7) = 3.55$, $P = 0.028$, $d_z = 1.26$) and biceps femoris (30%; $t(7) = 3.45$, $P = 0.032$, $d_z = 1.22$). In the ankle plantarflexor muscles, personalized assistance significantly reduced activation compared to the exo off condition, including the gastrocnemius lateralis (18%; $t(7) = 4.94$, $P = 0.005$, $d_z = 1.75$) and soleus (19%; $t(6) = 4.26$, $P = 0.016$, $d_z = 1.61$), whereas the corresponding reductions relative to the no exo condition were smaller and not significant (11%; $t(7) = 2.03$, $P = 0.247$, $d_z = 0.72$ and 15%; $t(6) = 2.18$, $P = 0.216$, $d_z = 0.82$). Muscle activation in the rectus femoris, vastus lateralis, tibialis anterior, and gastrocnemius medialis did not significantly change with personalized assistance compared to other conditions (Supplementary Fig. 1 and Supplementary Table 6).

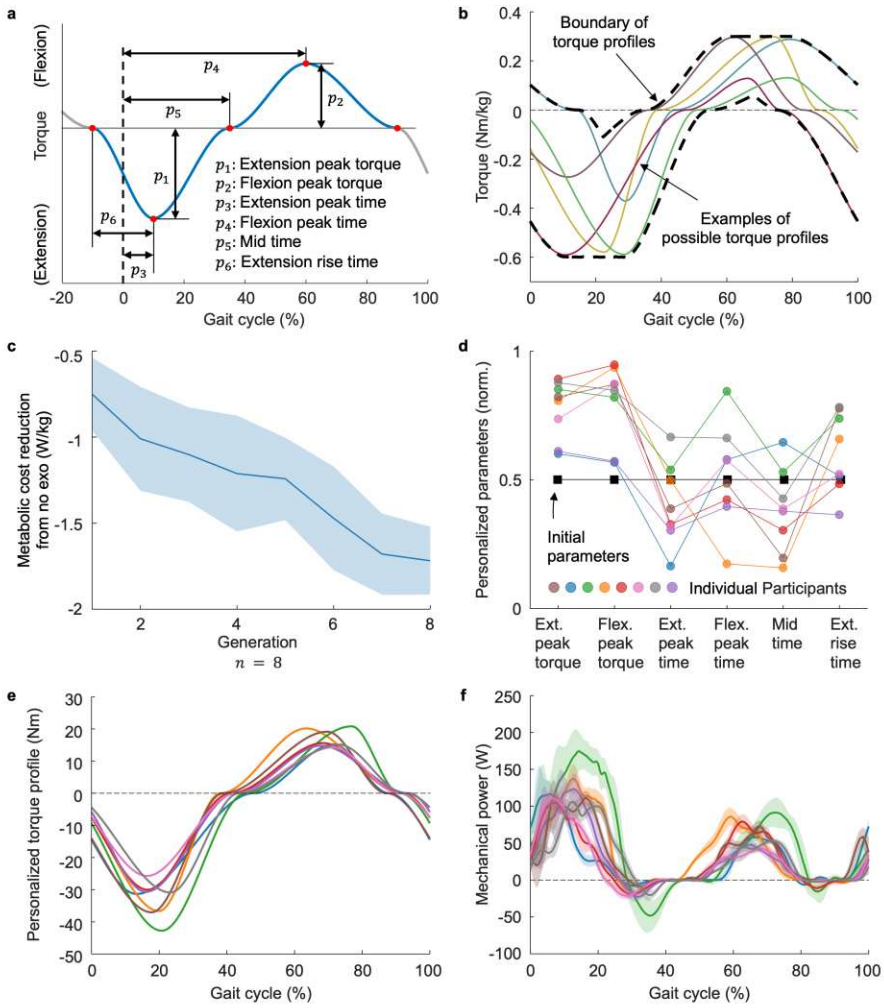


Fig. 4 | Human-in-the-loop optimization results. (a) The six parameters that define the magnitude and timing of the hip torque profile across the gait cycle. **(b)** Examples of possible torque profiles within the parameter boundaries used during optimization. **(c)** Each generation of

optimization had a progressively larger reduction in metabolic cost compared to the no exo condition. The line denotes the mean, and the shaded region indicates the standard error across participants. **(d)** Subject-specific personalized parameters normalized to the optimization boundaries for each parameter. **(e)** Subject-specific personalized hip torque profiles. **(f)** Subject-specific mechanical power profiles per leg provided by the exoskeleton during the subject-specific personalized assistance condition. Shaded regions indicate within-participant standard deviation.

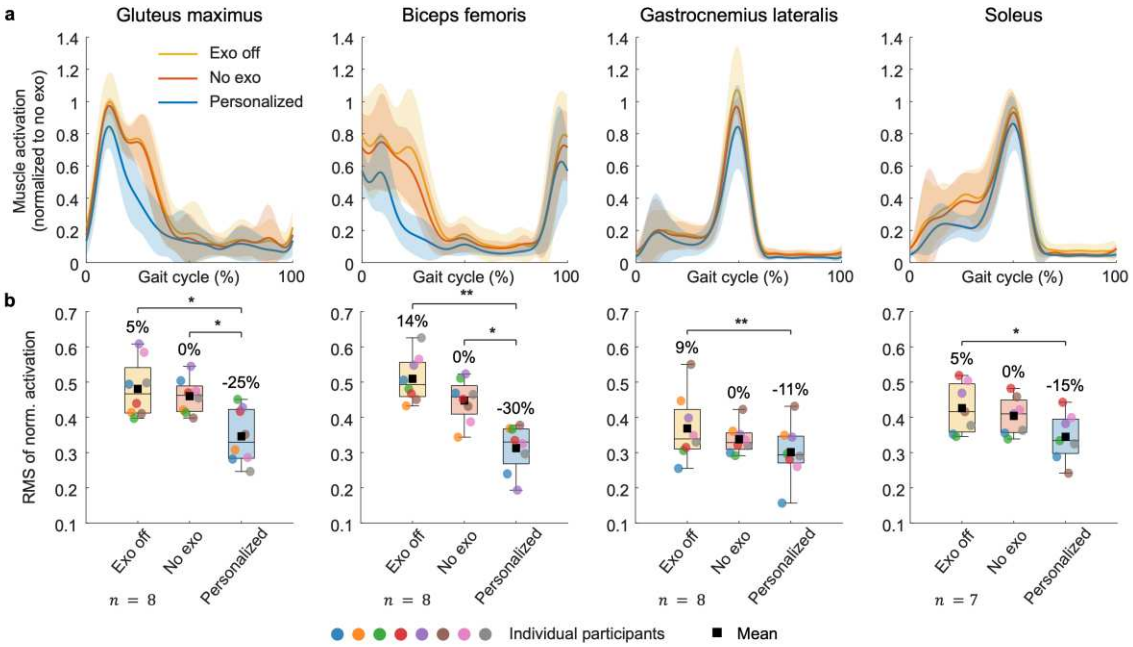


Fig. 5 | Lower-limb muscle activation across validation conditions during incline walking. **(a)** Muscle activation over the gait cycle for each validation condition (exo off, no exo, and personalized). For each muscle, activation was normalized to the peak magnitude in the no exo condition and then averaged across participants. Lines denote the mean and shaded regions indicate the standard deviation across participants. **(b)** The RMS (root-mean-square) of the mean normalized muscle activation across conditions with participant-level paired data. Boxes extend from the lower to upper quartiles, the center line indicates the median, and the whiskers extend from the minimum to the maximum data point. Pairwise comparisons were performed only where the repeated-measures ANOVA for that muscle was significant (*P < 0.05, **P < 0.01 after Bonferroni adjustment; see Methods).

During outdoor walking, personalized assistance reduced the cost of transport and increased speed compared to the no exo condition. Four participants who previously completed the indoor optimization protocol walked on uneven and inclined terrain (Fig. 6a) in the Blue Hills Reservation (Milton, MA, USA; Fig. 6b). Participants walked under the no exo and personalized assistance conditions in a randomized and double-reversal order (Supplementary Table 2). The route was 320 m long with a 10.3° incline and required approximately 6 minutes of walking (Fig. 6c). Personalized assistance reduced the cost of transport by 1.6 J/(m·kg) (20%; $t(3) = 5.97$, P = 0.009, 95% CI [0.74, 2.42], d_z = 2.98; Supplementary Table 4) and increased speed by 0.1 m/s

(9%; $t(3) = 2.55$, $P = 0.084$, $d_z = 1.28$; Supplementary Table 7) compared to the no exo condition (Fig. 6d). The cost of transport decreased in all four participants, but the paired differences did not meet the normality assumption of the *t*-test (Shapiro-Wilk $P = 0.04$), and a Wilcoxon signed-rank test cannot give a *P* value below 0.125 with four participants. The *t*-tests of this preliminary experiment are therefore reported descriptively (Supplementary Tables 4 and 7).

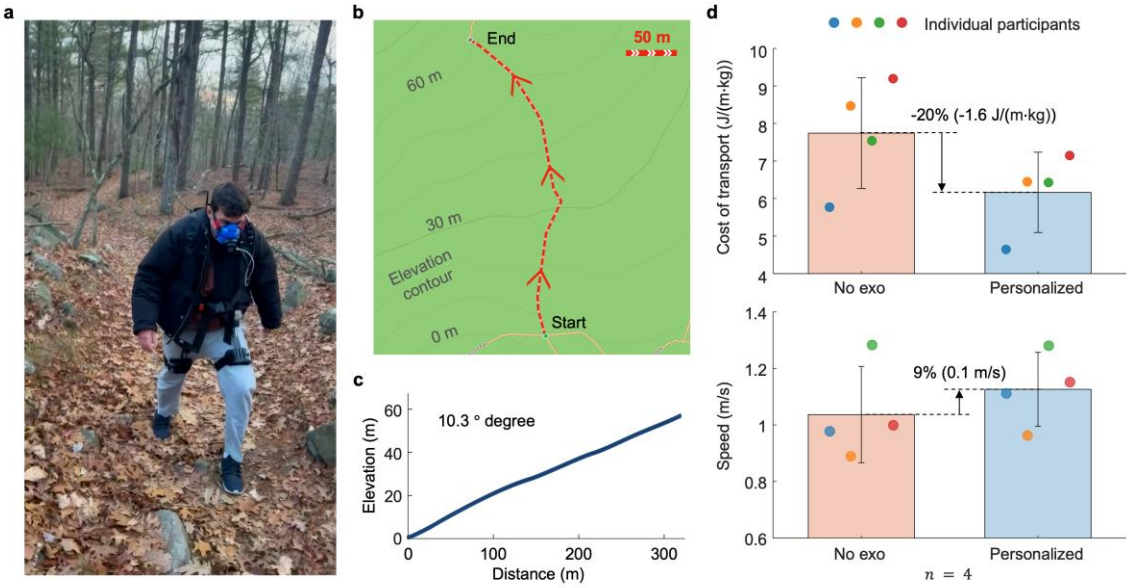


Fig. 6 | Outdoor validation on uneven and inclined terrain. (a) A participant walking outdoors on uneven terrain with personalized exoskeleton assistance. **(b)** Map of the outdoor route. **(c)** Elevation and distance along the outdoor route. The average incline was 10.3°. **(d)** The cost of transport (top) and speed (bottom) for the no exo and personalized assistance conditions. Whiskers indicate one standard deviation. Statistics for both outcomes (n = 4) are reported descriptively in Supplementary Tables 4 and 7.

Personalized exoskeleton assistance also reduced the cost of transport during a preliminary indoor load-carriage interval validation, a prolonged, intermittent walking task that was designed based on firefighter training protocols[32,33] and discussions with firefighters. Four participants walked on a treadmill at a 10° incline and 1 m/s while carrying a 21 kg load, completing five sets that alternated two minutes of walking with one minute of standing, and recording continued for five minutes after the final walking interval (Fig. 7a). The experiment was performed without the exoskeleton and with personalized assistance in a randomized, double-reversal order (Supplementary Table 2). Personalized assistance reduced the cost of transport across the protocol by 2.6 J/(m·kg) (20%; $t(3) = 8.10$, $P = 0.004$, 95% CI [1.60, 3.67], $d_z = 4.05$; Supplementary Table 4) compared with the no exo condition (Fig. 7b). Metabolic rate rose throughout each two-minute walking interval without reaching steady state and reached a higher value without the exoskeleton than with personalized assistance in every set (Fig. 7c). The respiratory exchange ratio was lower with personalized assistance than the no exo condition.

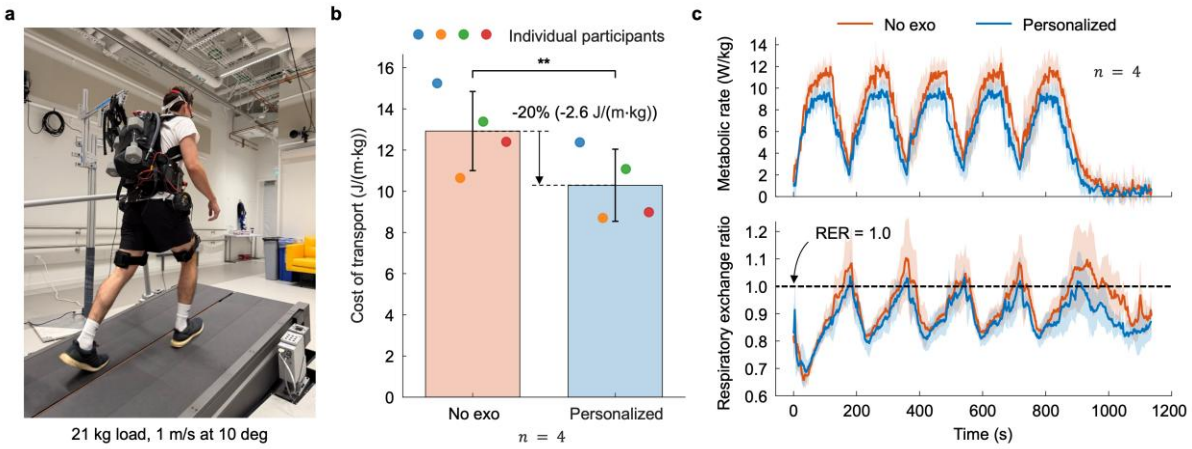


Fig. 7 | Indoor load-carriage interval validation. (a) A participant walking on the treadmill at a 10° incline and 1 m/s while carrying a 21 kg load and wearing the exoskeleton. **(b)** Cost of transport for the no exo and personalized assistance conditions, with individual participants shown as colored circles and whiskers indicating one standard deviation (paired *t*-test, $n = 4$, $^{**}P < 0.01$). **(c)** Metabolic rate (top) and respiratory exchange ratio (bottom) over the protocol for each condition. Lines denote the mean and shaded regions indicate the standard deviation across participants. The dashed line indicates a respiratory exchange ratio of 1.0, when carbon dioxide production equals oxygen consumption.

Discussion

The metabolic benefits provided by the hip exoskeleton were obtained with the combination of a device with a high power-to-mass ratio and effective assistance through personalization and training. The personalized assistance reduced the metabolic cost of incline walking by approximately the amount associated with removing a 40 kg backpack from the person during level ground walking[22], which we provide as an approximate reference for magnitude. The OpenHi-P exoskeleton motor and structural components were selected to provide an exoskeleton-side average positive mechanical power of 1.0 W/kg during incline walking (Supplementary Table 8), about 80% of the hip power of a tethered emulator at the same incline and speed (1.2 W/kg)[25] and 2.7 to 6.6 times that of prior portable exoskeletons (Fig. 2c). Normalized by the 4.97 kg worn mass of the device, this exoskeleton provides the largest mechanical power and absolute metabolic reduction per kilogram reported for a portable lower-limb exoskeleton in Supplementary Table 3. Most of this mass is carried proximally on the trunk and waist, where added mass has a smaller metabolic cost than mass carried distally on the limbs[22] (Supplementary Table 9). Human-in-the-loop optimization identified personalized assistance parameters to reduce metabolic cost. The multi-day optimization protocol also provided dedicated training time to allow users to adapt and become proficient using the device. Personalization and training also require a device capable of delivering sufficiently large assistance in each person's optimal range, but this study evaluated the three together and could not determine how much each contributed.

Participants may have achieved larger metabolic reductions with longer training and optimization time to benefit from higher magnitudes of assistance. We estimated that the torque magnitude provided by the portable exoskeleton (0.7 Nm/kg for extension) should be slightly lower

than the personalized hip assistance (0.9 Nm/kg for extension) from a multi-joint exoskeleton emulator study[25]. This assumed that the prior study benefited from higher hip assistance by assisting multiple joints, providing ankle and knee support we could not provide with a single-joint hip exoskeleton, and by compensating for the heavier exoskeleton emulator weight. During piloting, we adjusted the initial torque magnitude parameters (0.4 Nm/kg for extension) and boundaries (0.2 to 0.6 Nm/kg for extension) based on user comfort and to account for the fact that users will likely adapt to benefit from higher torque[24] as they are trained with the device throughout the optimization protocol. However, most participants' peak torque parameters approached the parameter boundaries and were continuing to increase in magnitude by the final generation of optimization (Fig. 4d, Supplementary Fig. 2). This suggests that participants did not reach a steady-state, optimal set of parameters within 8 generations and may have benefited from higher torque. Optimal torque magnitude continued to increase with user training time in an ankle exoskeleton study[24], even after 5 hours, supporting the idea that participants may benefit from additional training beyond the 3 hours provided in this study. Future studies could expand the parameter search space and increase both the optimization and training time to better explore high torque magnitudes and potentially achieve larger metabolic reductions.

Personalized assistance was associated with reduced activation in muscles that did not span the hip compared to the exo off condition, suggesting that users may reconfigure whole-limb coordination with hip assistance. Although the exoskeleton primarily applies torque at the hip to support muscles around the targeted joint, hip assistance can influence knee and ankle mechanics through inter-joint coupling within the lower limb[34]. The mechanical or neural mechanism of this reduction remains unresolved and would require lower-limb kinematics and an inverse-dynamics analysis to establish. We also expected hip assistance to reduce knee extensor activation because hip extension can support knee extension during the stance phase[35]. We did not observe a significant change in these muscles, and previous work has reported an increase in vastus lateralis activation with hip assistance, so this response is difficult to attribute to a single mechanism.

Experimental evidence of large metabolic benefits across physically demanding walking conditions, together with the open-source release of the device, supports future translational research with the OpenHi-P exoskeleton. Few portable exoskeletons have demonstrated mobility improvements on real-world terrain[17,36,37], making this an important milestone to highlight how exoskeletons can provide benefits beyond the laboratory. The preliminary results from the outdoor experiment highlight how the OpenHi-P exoskeleton is capable of providing benefits for metabolic cost in naturalistic environments (Fig. 6). While the outdoor path was selected to have a similar incline to the treadmill study, the slope was not constant and included varied and rocky terrain, which resembles the uneven ground encountered during outdoor occupational work. The preliminary indoor load-carriage interval validation further suggested that assistance can be sustained across repeated bouts of high-intensity effort over a prolonged work period. The cost of transport in this validation is an estimate, because it was computed from gas exchange during a protocol that did not reach a metabolic steady state and its 5-min recovery window captured only part of the post-exercise recovery. Ending the integration at the final walking interval changed the reduction with personalized assistance from 20.3% to 18.7% (group-mean curves in Fig. 7c). Further development and testing are needed to determine if these mobility benefits can be provided for workers with physically intensive jobs. To facilitate this translation, the OpenHi-P

exoskeleton was developed as an open-source platform to allow other researchers and clinicians to replicate and modify the system. We hope that these resources, along with other open-source efforts in the exoskeleton community[38,39], will reduce the time required to develop exoskeletons, improve study reproducibility, and facilitate translation of these technologies.

The OpenHi-P exoskeleton reduced the metabolic cost of incline walking by approximately twice the largest reduction previously reported for a portable lower-limb exoskeleton in studies of healthy adults that met our inclusion criteria. Preliminary experiments suggested that effective assistance extends to walking on real-world inclined terrain and to carrying a load across repeated bouts of high-intensity effort. Researchers can leverage this conceptual framework for exoskeleton development by selecting capable hardware, personalizing assistance, and training users to inform future portable exoskeletons that maximize mobility benefits for different applications. Researchers and clinicians could directly use and adapt this open-source hardware and software hip exoskeleton platform to accelerate exoskeleton research and explore how to achieve large metabolic benefits during incline walking and related tasks indoors and in real-world terrain. Whether these benefits extend to physically demanding occupations remains to be determined and would require testing over longer durations, with occupationally representative loads and tasks, in more representative cohorts. Together, the OpenHi-P exoskeleton and results provide an accessible and capable platform that could accelerate the translation of exoskeletons to address health risks for occupations involving physically demanding activity.

Methods

OpenHi-P exoskeleton hardware design

We developed an open-source hip exoskeleton that combines a comfortable soft interface with reinforced rigid structural elements to enable high-torque assistance. We adopted the initial design from the M-Blue hip exoskeleton[39] and reinforced key load-bearing regions with rigid components to efficiently transmit motor-generated power to the torso and thigh. A rigid back piece coupled bilateral hip actuation modules to reduce undesired device rocking relative to the body by compensating for any asynchronous hip joint torques applied to each leg. The effective moment arm was individualized for each participant by adjusting the rigid back and thigh struts, which improved fit and reduced soft textile deformation and interface pressure on the body.

We fabricated the hip exoskeleton using a commercially available interface and custom-designed carbon-fiber and aluminum components. We used an off-the-shelf vest (Padded Nylon Straps, Smith Performance Sprayers) and hip brace (T-scope, Breg) as our exoskeleton interface to maximize user comfort and ensure the fit across participants. The waist frame and thigh strut were fabricated from molded carbon-fiber composites to achieve high stiffness at low mass. Carbon-fiber sheets were laid onto a 3D-printed mold, coated with epoxy, and cured overnight. Additional 2D components were waterjet-cut from carbon-fiber or aluminum sheets. A step-by-step fabrication process and additional build details are provided in a supporting document.

A high torque density brushless motor (AK10-9, Cubemars) was selected to explore a wide range of assistive torques during incline walking. A previous emulator-based study reported that peak hip extension torque magnitudes approached a comfort-based limit of 0.9 Nm/kg during 10° incline walking at 1 m/s[25]. Given that the emulator system weighed 13.5 kg and provided multi-joint assistance, we expected that the optimal hip torque magnitude required from a portable

exoskeleton that only assisted the hip joint would be lower. We therefore selected the available commercial motor that most closely matched these torque requirements, providing 48 Nm peak torque, corresponding to approximately 0.7 Nm/kg for 70 kg participants. The motor weighs 0.96 kg and contains a 9:1 ratio planetary gearbox, remaining backdrivable to minimize the impedance to the user during the exo off condition. The device is powered by a 6-cell 3250 mAh lithium-polymer battery (450 g, 75 Wh), which supports approximately 40 minutes of continuous assisted walking at the assistance magnitudes based on motor currents recorded across participants (Supplementary Fig. 3).

The exoskeleton directly measured joint torque applied to the hip rather than inferring it from motor current, reducing model-mismatch errors and enabling reliable torque control to provide a more consistent assistance. Although several previous studies have used the motor current calibrated in the benchtop test to estimate torque, the torque applied to the user can differ due to transmission efficiency and compliance in the wearable interface[40]. A single-point, low-profile load cell (S230, Strain Measurement Devices) was used to accurately measure the hip torque applied with the exoskeleton. We selected an 18 kg capacity single-point load cell to cover the maximum torque of 48 Nm and implemented it in the thigh interface. We calibrated the torque using a benchtop setup with a reference torque sensor (TFF350, Futek; Supplementary Fig. 4). This direct torque measurement enables closed-loop control of the applied torque, rather than the open-loop control from a current-torque relationship used in previous portable exoskeletons. The relationship between motor current and torque also depends on the rate at which torque is applied, which we characterized with the exoskeleton worn during standing and a target torque of 43 Nm applied repeatedly at a slower and a faster rate. Using the relationship measured at one rate to predict the torque at the other rate produced substantial errors, confirming that motor current alone is not a reliable estimate of the torque delivered in this high-torque regime (Supplementary Fig. 5).

Open-source exoskeleton controller

We developed an open-source embedded software to control the hip exoskeleton. A microcontroller (STM32F4, STMicroelectronics) read and processed sensor data and controlled the motor in real-time through Controller Area Network (CAN) bus. The gait cycle was continuously estimated using a thigh-mounted IMU (MTi-3, Xsens) on the exoskeleton to construct a sagittal-plane phase portrait from the thigh angle and angular velocity[41]. Using phase variables from a thigh-mounted IMU is more reliable than phase estimates derived from motor encoder data due to trunk motion and exoskeleton-induced kinematic artifacts. The gait cycle was linearized in the time domain using the stride frequency estimated from the phase portrait to generate the desired torque profile without temporal misalignment.

A desired torque profile defined by six parameters was prescribed as a function of the gait cycle. The controller evaluated the desired torque corresponding to the instantaneous gait cycle and commanded the motor to track this phase-dependent torque value. A motor current command was computed as the sum of a feedforward term, a proportional feedback term on the torque tracking error between the desired and measured torque, and a proportional damping term on the motor velocity. The resulting closed-loop command was sent to the motor driver electronics via CAN.

A separate PC was used to optimize the assistance by collecting the metabolic cost data and sending the hip torque parameters to the exoskeleton controller through Bluetooth communication. We used the covariance matrix adaptation evolutionary strategy (CMA-ES) algorithm to optimize six hip torque parameters[42]. A Python script captured time-synced oxygen and carbon dioxide exchange from the COSMED software and computed energy expenditure in real time. The optimizer (CMA-ES) ranked candidate conditions (parameter sets) in order of estimated metabolic cost and updated the search distribution to generate new candidate conditions. The first candidate condition returned by the optimizer in each generation was replaced with the best-performing condition of the previous generation, or with the initial guess (Supplementary Table 5) in the first generation, which may help optimization by providing previously beneficial conditions. Nine candidate conditions within each generation were ordered from smaller to larger based on the average of extension and flexion torque magnitudes to help users adapt to assistance across conditions, and their costs were returned to the optimizer in the same order. The optimizer adapted its step size with two-point step-size adaptation (TPA), which compares the costs of the first two candidates of each generation. Each condition with six parameters was then sent to the exoskeleton controller via Bluetooth, which regenerated the desired torque profile accordingly.

Experimental design

Participants completed a multi-day experimental protocol to optimize and validate the hip assistance during incline walking. All experiments were conducted under Harvard institutional review board approval and included human subject experiments in both laboratory and outdoor settings (IRB23-0435). Eight participants were recruited and provided written informed consent before completing the protocol. We set the optimization to eight generations to balance allowing sufficient time for convergence while maintaining experimental feasibility. Each generation consisted of nine conditions, determined by the number of parameters to optimize[42] from the six parameters in our study. Depending on the participant's fatigue level, the protocol was completed over 2 or 3 days. Each participant's optimization was a single CMA-ES optimization that was continued across days from the optimizer log. The three validation conditions were each performed twice in a randomized, double-reversal sequence (ABCCBA), giving six 5-minute bouts per participant (Supplementary Table 2). The double reversal was used to counterbalance ordering and time-varying effects. The exo off condition, in which the exoskeleton was worn but fully unpowered, was included to account for the effect of wearing the device without assistance.

The outdoor validation was conducted on a real-world incline terrain with a subset of the participants that completed the indoor optimization protocol. The outdoor route was selected during a prior visit to the site so that participants could ascend a consistent average slope continuously for five to six minutes. All sessions were conducted in clear weather. Participants were asked to wear comfortable shoes and to walk at a self-selected speed. Participants first walked the path without the exoskeleton to become familiar with the terrain. After each ascent, participants returned to the starting point and rested as long as they needed before the next condition.

For the indoor load-carriage interval validation, participants walked on a treadmill at a 10 degree incline and 1 m/s while carrying a 21 kg load in addition to the exoskeleton. The load approximates the mass of full firefighting protective equipment, including turnout gear and a self-

contained breathing apparatus[33], and the intermittent work-rest structure follows protocols used to reproduce fireground physiological demands[32]. The protocol consisted of five sets of two minutes of walking followed by one minute of standing. Metabolic data were recorded continuously and collection continued for five minutes after the end of the final walking interval to include the recovery following the task, and the outcome measure was the cost of transport computed from the start of the protocol to the end of that recovery window. A five-minute quiet standing measurement with the same load was collected at the start of each session as a reference. Two conditions were compared, carrying the load without the exoskeleton and carrying the load while the exoskeleton provided the personalized assistance identified for that participant during the indoor optimization, so that the mass and impedance penalty of wearing the device is included in the reported benefit. Each condition was measured twice within a single session in a randomized double-reversal order and averaged, with ten minutes of rest between consecutive bouts. Participants in the outdoor validation and indoor load-carriage interval validation were restricted to those who had completed the multi-day indoor optimization protocol, because each condition used that participant's personalized assistance.

Data collection and processing

Metabolic cost was measured using a portable respirometry equipment (K5, COSMED). Participants wore a metabolic mask, and respiratory data were recorded breath-by-breath. Metabolic cost (energy expenditure in watts) was computed from the volumetric change of oxygen and carbon dioxide for each breath using the Brockway equation[43]. The metabolic cost of quiet standing was subtracted from the gross values to isolate the net metabolic cost of walking. During the optimization, steady-state metabolic rate was estimated for each 2-min condition by fitting a first-order exponential model after excluding the first five breaths to reduce transient and delay effects. During the indoor validation, steady-state metabolic rate was calculated by averaging the last 2 minutes of each 5-min condition. For the outdoor validation and the indoor load-carriage interval validation, the cost of transport was computed by integrating the metabolic cost over the entire measurement period using the trapezoidal rule and dividing by the total distance walked. Respirometry data were recorded continuously from the start of the protocol until the end of the post-walk recovery period, which was 2 minutes outdoors and 5 minutes for the load-carriage protocol. For the outdoor validation, walking distance was measured three times at random during the experiment using a portable distance measure (DigiRoller, Calculated Industries) and averaged, and the elevation profile was captured using a mapping tool (onthegomap). For the indoor load-carriage interval validation, walking distance was calculated by multiplying the walking speed and the total duration of walking. The respiratory exchange ratio was computed for each breath as the ratio of carbon dioxide production to oxygen consumption.

Muscle activation was recorded using surface electromyograph (EMG) sensors (Trigno, Delsys). Sixteen EMG sensors were placed bilaterally on eight lower-limb muscles (gluteus maximus, rectus femoris, vastus lateralis, biceps femoris, tibialis anterior, gastrocnemius medialis, gastrocnemius lateralis, and soleus) following the sensor placement guideline[44]. For each participant and muscle, the EMG of a single leg was analyzed, and the same leg was used in all validation conditions so that every condition was compared on the same channel; if the signal of one leg was lost in any condition, the other leg was used for that muscle in all conditions. Raw EMG signals were band-pass filtered using a 4th-order Butterworth filter (15-380 Hz), full-wave

rectified, and then low-pass filtered using a 4th-order Butterworth filter (7 Hz) to obtain the linear envelope. Ground reaction forces were simultaneously collected using an instrumented treadmill (Bertec) and used to segment the EMG signal into gait cycles. Muscle activation was analyzed over the last 2 minutes of each 5-minute bout, matching the window used for metabolic rate. All channels were visually inspected for signal loss before analysis and processed identically, and no strides or data segments were excluded. A muscle was excluded only if each leg lost its signal in at least one condition, which occurred for the soleus in one participant; the effective sample size is therefore seven participants for the soleus and eight participants for every other muscle. Each muscle activation within the subject was normalized to its peak activation in the no exo condition. Normalized muscle activations were then group-averaged across participants for each exoskeleton condition. Due to inter-participant variability in activation timing, group-averaging reduced peak magnitudes, resulting in a peak value for the no exo condition that fell below 1. Participant-level root-mean-square values (Fig. 5b and Supplementary Fig. 1b) and the individual-participant activation profiles for every muscle and condition are provided in Supplementary Data 1.

Mechanical power was computed from hip torque and motor angular velocity, which were recorded by the exoskeleton microcontroller. The raw torque was low-pass filtered offline using a third-order Butterworth filter (8 Hz; MATLAB filtfilt) to remove high-frequency noise. Instantaneous mechanical power was calculated for each stride as the product of filtered hip torque (Nm) and motor angular velocity (rad/s) and averaged across strides at each percent of the gait cycle. Average positive mechanical power per leg was computed by averaging the stride-averaged power over the whole gait cycle with negative values set to zero (positive work per stride divided by stride duration) and normalized by body mass. The value for both legs was taken as twice the right-leg value, assuming bilateral symmetry. We report this quantity as exoskeleton-side positive mechanical power, computed from the torque and angular velocity measured on the exoskeleton.

Statistical analysis

Sample size was planned for a single primary outcome, the net metabolic rate during indoor incline walking with personalized assistance compared to the no exo condition, and each subsequent experiment was sized separately for its own primary outcome. We conducted a power analysis based on previously reported metabolic rate values showing the best-performing metabolic reduction with a portable exoskeleton[17]. This analysis used a power of $1 - \beta = 0.8$ and a significance level of $\alpha = 0.05$. The difference in mean metabolic rate between personalized assistance and normal walking was 1.08 W/kg, and the standard deviation of the within-subject differences was 0.34 W/kg. This analysis indicated that a minimum sample size of $n = 4$ participants would be sufficient for the planned experiments. We recruited $n = 8$ participants to provide a conservative margin for potential data loss. The sample sizes for the outdoor validation and indoor load-carriage interval validation were determined before their first session based on the metabolic result of the indoor validation, which gave a mean difference of 2.06 W/kg with a standard deviation of the paired differences of 0.70 W/kg, corresponding to $d_z = 2.96$. Assuming that assistance would reduce metabolic cost, a one-sided calculation required $n = 3$ participants, whereas a two-sided calculation required $n = 4$. We recruited four participants for each of the outdoor and load-carriage validations. We used the indoor results because they provided the only available effect-size estimate for this device and assistance, although this effect size may not be

directly applicable to the two cost-of-transport (COT) outcomes, which integrate non-steady-state gas exchange during walking and recovery. The indoor muscle activation analyses, the outdoor walking speed comparison, and the respiratory exchange ratio from the indoor load-carriage interval validation were treated as secondary outcomes that were not included in the sample-size calculation and are reported as exploratory analyses.

Statistical analyses of differences between conditions were performed using within-participant methods with a significance level of $\alpha = 0.05$. We performed all analyses using MATLAB and built-in statistical functions (MathWorks). Repeated bouts of the same condition were averaged to give one value per condition per participant. Normality of the within-participant differences was assessed with the Shapiro-Wilk test prior to the comparisons. Where normality was violated, the unadjusted P value of a Wilcoxon signed-rank test is reported alongside the paired *t*-test for the seven- and eight-participant comparisons, and sensitivity analyses were used instead for the four-participant comparisons. Sphericity across the three indoor conditions was assessed with Mauchly's test. Where sphericity was violated, the Greenhouse-Geisser correction was applied. All *P* values are two-sided, and every comparison is reported with the test statistic, its degrees of freedom, the *P* value, the 95% confidence interval of the mean difference, and a standardized effect size. *P* values reported in the text are Bonferroni-adjusted where post hoc comparisons were performed across the three conditions, and unadjusted exact values for each paired comparison, together with confidence intervals for the muscle activation comparisons, are given in Supplementary Tables 4 and 6.

For the indoor validation including three conditions (exo off, no exo, and personalized assistance), a repeated-measures analysis of variance (ANOVA) was first conducted to test for a main effect of condition. When a significant main effect was observed, planned post hoc pairwise comparisons were performed using paired *t*-tests with Bonferroni correction to account for multiple comparisons. For the muscle activation comparisons in this experiment, a repeated-measures ANOVA was evaluated for each muscle, and pairwise comparisons were performed only where that ANOVA was significant, with Bonferroni adjustment within the three comparisons of that muscle (Supplementary Table 6). No multiplicity adjustment was made across muscles for the eight ANOVAs or the pairwise comparisons. The outdoor validation and indoor load-carriage interval validation each involved two conditions (no exo and personalized assistance), and differences were assessed using paired *t*-tests. With four participants, a rank-based test cannot reach significance regardless of the size of the effect. We therefore performed sensitivity analyses, using a leave-one-out analysis, in which the comparison was recomputed with each participant omitted in turn, and percentile bootstrap confidence intervals from 10,000 resamples of the paired differences. Both analyses are reported for each of these experiments in Supplementary Table 4.

For each assistance parameter, values were averaged within each generation for every participant and normalized to the search bounds, so that 0 and 1 correspond to the lower and upper bound of the range explored by the optimizer. Pooled participant-by-generation values were fitted with a single-rate exponential model, $y = a + a_0 e^{-wg}$, where g is the generation number, a is the steady-state value, a_0 is a scaling factor, and w is the rate constant, whose inverse is the characteristic number of generations over which the parameter changed[24]. Model parameters were estimated using unweighted nonlinear least squares, and the fitted curves are shown in Supplementary Fig. 2 for description only. Trends were tested at the participant level because the pooled values included repeated observations from each participant. The slope of each

participant's normalized values across generations was computed for each parameter by linear regression, and the eight slopes were tested against zero with a one-sample *t*-test (Bonferroni-adjusted across the six parameters) and an exact sign test. Where a trajectory had not saturated within the tested generations, w is not identifiable and we report the direction and consistency of the trend instead.

Comparison to other portable exoskeletons

We compared the benefits of the OpenHi-P exoskeleton with the best results of comparable previous studies using portable exoskeletons (Supplementary Table 3 and Supplementary Fig. 6). We define a portable exoskeleton as an untethered, autonomous system in which actuation, sensing, computation, and power are carried on the body, without any requirement on device mass. Tethered emulators achieve large metabolic reductions[25,34] but are not included in the comparison because their actuation, power, and computation are not carried by the wearer. We considered only studies that reported metabolic reductions compared to the no exo condition and provided a benefit to the user for direct comparison. We also limited our comparisons to studies with at least five participants, as results from smaller samples can be noisy due to measurement error and individual variability. The hip configuration of OpenExo is listed for reference, but was excluded from the direct comparison because its reported values come from two participants. We further limited the comparison to healthy adults walking without a gait aid such as a handrail, cane, or walker, because a gait aid changes the mechanical demand of the task and prevents a direct comparison of assistance magnitude. For Fig. 2b, we selected the studies that reported the absolute metabolic reduction and evaluated assistance during stair climbing, incline walking, or walking with a payload, which reflect the physically demanding tasks. For Fig. 2c, we selected the studies that reported the average positive mechanical power and the absolute metabolic reduction. We compared only exoskeleton power during walking, which was computed from the torque measured or estimated from the exoskeleton and is distinct from the nominal power rating of the motors. The line in Fig. 2c is a least-squares linear fit through the origin to the prior portable exoskeletons (slope 1.6).

We used the absolute metabolic reduction as the primary comparison metric because our objective was to provide assistance during physically demanding activities. An exoskeleton that provides low assistance during a less demanding task could achieve a high percentage reduction in metabolic cost while delivering a small absolute reduction, because the percentage reduction is normalized to the baseline cost of the task. Where a study reported only the percentage reduction, we derived the absolute reduction from the reported metabolic rate and the baseline metabolic cost.

Data availability: The participant-level data are provided in Supplementary Data 1, in the file study_data.mat (MATLAB format), together with a README that describes its contents and the analysis scripts (see Code availability). Participant information, individual results and the values from prior studies are also provided in Supplementary Tables 1, 8 and 3. Source data are provided with this paper.

Code availability: The code and hardware design files are in the OpenHi-P-Exo repository (https://github.com/Harvard-Slade-Lab/OpenHi-P-Exo). Release v1.0.0, which accompanies this paper, is archived at Zenodo (https://doi.org/10.5281/zenodo.24250121) and contains the exoskeleton firmware, the human-in-the-loop optimization software, and the hardware design files and build guide under the MIT License, with third-party components under their own licenses. The analysis scripts are provided with the data in Supplementary Data 1.

Acknowledgments: We thank A. Chin, D. Locurto, C. Rodriguez, and L. Gallezot for assistance with data collection; the Slade Lab members for editorial suggestions; M. Cooper, S. Canete, T. Hoang, and C. Walsh for technical support during exoskeleton development; and S. Delp for feedback on the project. This study was supported by Kempner Institute for the Study of Natural & Artificial Intelligence at Harvard University and the Raj Bhattacharyya and Samantha Heller Assistive Technology Initiative Fund.

Author contributions: J.R.C. contributed to conceptualization, methodology, investigation, visualization, and writing. Y.D. contributed to methodology, investigation, and visualization. C.R. contributed to investigation and visualization. P.S. contributed to conceptualization, methodology, visualization, and writing.

Competing interests: The authors declare no competing interests.

References

1. United States Firefighter Injuries. https://www.nfpa.org/education-and-research/research/nfpa-research/fire-statistical-reports/firefighter-injuries-in-the-united-states.
2. Isaacson, B. *et al.* Lower Extremity musculoskeletal injuries in United States active duty service members: Prevalence/incidence, health care utilization, and cost analysis spanning fiscal years 2016-2021. *Mil. Med.* **189**, 56–69 (2024).
3. Montgomery, J. R. & Grabowski, A. M. The contributions of ankle, knee and hip joint work to individual leg work change during uphill and downhill walking over a range of speeds. *R. Soc. Open Sci.* **5**, 180550 (2018).
4. Walsh, G. S. & Low, D. C. Military load carriage effects on the gait of military personnel: A systematic review. *Appl. Ergon.* **93**, 103376 (2021).
5. Punaxallio, A., Lusa, S. & Luukkonen, R. Protective equipment affects balance abilities differently in younger and older firefighters. *Aviat. Space Environ. Med.* **74**, 1151–1156 (2003).
6. Park, K., Rosengren, K. S., Horn, G. P., Smith, D. L. & Hsiao-Wecksler, E. T. Assessing gait changes in firefighters due to fatigue and protective clothing. *Saf. Sci.* **49**, 719–726 (2011).
7. Mooney, L. M., Rouse, E. J. & Herr, H. M. Autonomous exoskeleton reduces metabolic cost of human walking during load carriage. *Journal of NeuroEngineering and Rehabilitation* **11**, 80 (2014).
8. Mooney, L. M., Rouse, E. J. & Herr, H. M. Autonomous exoskeleton reduces metabolic cost of human walking. *Journal of NeuroEngineering and Rehabilitation* **11**, 151 (2014).
9. Mooney, L. M. & Herr, H. M. Biomechanical walking mechanisms underlying the metabolic reduction caused by an autonomous exoskeleton. *Journal of NeuroEngineering and Rehabilitation* **13**, 4 (2016).

10. Seo, K., Lee, J., Lee, Y., Ha, T. & Shim, Y. Fully autonomous hip exoskeleton saves metabolic cost of walking. in *2016 IEEE International Conference on Robotics and Automation (ICRA)* 4628–4635 (IEEE, 2016).
11. Seo, K., Lee, J. & Park, Y. J. Autonomous hip exoskeleton saves metabolic cost of walking uphill. in *2017 International Conference on Rehabilitation Robotics (ICORR)* 246–251 (IEEE, 2017).
12. Kim, J. *et al.* Reducing the metabolic rate of walking and running with a versatile, portable exosuit. *Science* **365**, 668–672 (2019).
13. Molinaro, D. D., Kang, I. & Young, A. J. Estimating human joint moments unifies exoskeleton control, reducing user effort. *Sci Robot* **9**, eadi8852 (2024).
14. Panizzolo, F. A. *et al.* A biologically-inspired multi-joint soft exosuit that can reduce the energy cost of loaded walking. *Journal of NeuroEngineering and Rehabilitation* **13**, 43 (2016).
15. Kim, D.-S. *et al.* A wearable hip-assist robot reduces the cardiopulmonary metabolic energy expenditure during stair ascent in elderly adults: a pilot cross-sectional study. *BMC Geriatrics* **18**, 230 (2018).
16. Cao, W., Chen, C., Hu, H., Fang, K. & Wu, X. Effect of hip assistance modes on metabolic cost of walking with a soft exoskeleton. *IEEE Trans. Autom. Sci. Eng.* **18**, 426–436 (2021).
17. Slade, P., Kochenderfer, M. J., Delp, S. L. & Collins, S. H. Personalizing exoskeleton assistance while walking in the real world. *Nature* **610**, 277–282 (2022).
18. Xu, Y. *et al.* A portable soft exosuit to assist stair climbing with hip flexion. *Electronics (Basel)* **12**, 2467 (2023).
19. Park, D., An, J., Lee, D., Kang, I. & Young, A. J. Human-in-the-Loop Optimization of Hip Exoskeleton Assistance During Stair Climbing. *IEEE Trans Biomed Eng* **72**, 2147–2156 (2025).
20. Jackson, R. W. & Collins, S. H. An experimental comparison of the relative benefits of work

and torque assistance in ankle exoskeletons. *J. Appl. Physiol.* **119**, 541–557 (2015).

21. Kang, I., Hsu, H. & Young, A. The effect of hip assistance levels on human energetic cost using robotic hip exoskeletons. *IEEE Robot. Autom. Lett.* **4**, 430–437 (2019).
22. Browning, R. C., Modica, J. R., Kram, R. & Goswami, A. The effects of adding mass to the legs on the energetics and biomechanics of walking. *Med. Sci. Sports Exerc.* **39**, 515–525 (2007).
23. Slade, P. *et al.* On human-in-the-loop optimization of human-robot interaction. *Nature* **633**, 779–788 (2024).
24. Poggensee, K. L. & Collins, S. H. How adaptation, training, and customization contribute to benefits from exoskeleton assistance. *Sci. Robot.* **6**, eabf1078 (2021).
25. Franks, P. W. *et al.* The Effects of Incline Level on Optimized Lower-Limb Exoskeleton Assistance: A Case Series. *IEEE Trans Neural Syst Rehabil Eng* **30**, 2494–2505 (2022).
26. Bryan, G. M., Franks, P. W., Klein, S. C., Peuchen, R. J. & Collins, S. H. A hip–knee–ankle exoskeleton emulator for studying gait assistance. *Int. J. Rob. Res.* **40**, 722–746 (2021).
27. Witte, K. A., Zhang, J., Jackson, R. W. & Collins, S. H. Design of two lightweight, high-bandwidth torque-controlled ankle exoskeletons. in *2015 IEEE International Conference on Robotics and Automation (ICRA)* 1223–1228 (IEEE, 2015).
28. Zhang, J. *et al.* Human-in-the-loop optimization of exoskeleton assistance during walking. *Science* **356**, 1280–1284 (2017).
29. Tan, G. R. & Collins, S. H. Design of an ankle exoskeleton with twisted string actuation for running assistance. *Wearable Technol.* **6**, e34 (2025).
30. Miller, D. E., Tan, G. R., Farina, E. M., Sheets-Singer, A. L. & Collins, S. H. Characterizing the relationship between peak assistance torque and metabolic cost reduction during running with ankle exoskeletons. *Journal of NeuroEngineering and Rehabilitation* **19**, 46 (2022).
31. Nuckols, R. W. *et al.* Mechanics of walking and running up and downhill: A joint-level

perspective to guide design of lower-limb exoskeletons. *PLoS One* **15**, e0231996 (2020).

32. Abel, M. G., Mortara, A. J. & Pettitt, R. W. Evaluation of circuit-training intensity for firefighters. *J. Strength Cond. Res.* **25**, 2895–2901 (2011).
33. Gonzalez, D. E., Waldman, H. S. & McAllister, M. J. The metabolic and physiological demands of a simulated fire ground test versus a live-fire training evolution in professional firefighters. *Int. J. Exerc. Sci.* **16**, 230–241 (2023).
34. Franks, P. W. *et al.* Comparing optimized exoskeleton assistance of the hip, knee, and ankle in single and multi-joint configurations. *Wearable Technol.* **2**, e16 (2021).
35. Ding, Y. *et al.* Effect of timing of hip extension assistance during loaded walking with a soft exosuit. *Journal of NeuroEngineering and Rehabilitation* **13**, 87 (2016).
36. Tricomi, E. *et al.* Soft robotic shorts improve outdoor walking efficiency in older adults. *Nat. Mach. Intell.* **6**, 1145–1155 (2024).
37. Bowersock, C. D. & Lerner, Z. F. Feasibility of using autonomous ankle exoskeletons to augment community walking in cerebral palsy. *IEEE Open J. Eng. Med. Biol.* **6**, 75–81 (2025).
38. Williams, J. R. *et al.* OpenExo: An open-source modular exoskeleton to augment human function. *Sci. Robot.* **10**, eadt1591 (2025).
39. Nesler, C., Thomas, G., Divekar, N., Rouse, E. J. & Gregg, R. D. Enhancing Voluntary Motion with Modular, Backdrivable, Powered Hip and Knee Orthoses. *IEEE Robot Autom Lett* **7**, 6155–6162 (2022).
40. Cooper, M. *et al.* Design & systematic evaluation of power transmission efficiency of an ankle exoskeleton for walking post-stroke. in *2024 IEEE International Conference on Robotics and Automation (ICRA)* 5526–5532 (IEEE, 2024).
41. Quintero, D., Lambert, D. J., Villarreal, D. J. & Gregg, R. D. Real-time continuous gait phase and speed estimation from a single sensor. in *2017 IEEE Conference on Control Technology and Applications (CCTA)* 847–852 (IEEE, 2017).

42. Hansen, N. The CMA evolution strategy: a comparing review. in *Towards a New Evolutionary Computation* (eds Lozano, J. A., Larrañaga, P., Inza, I. & Bengoetxea, E.) 75–102 (Springer, 2006).
43. Brockway, J. M. Derivation of formulae used to calculate energy expenditure in man. *Hum. Nutr. Clin. Nutr.* **41**, 463–471 (1987).
44. Hermens, H. J., Freriks, B., Disselhorst-Klug, C. & Rau, G. Development of recommendations for SEMG sensors and sensor placement procedures. *J. Electromyogr. Kinesiol.* **10**, 361–374 (2000).

Supplementary Files

This is a list of supplementary files associated with this preprint. Click to download.

- SourceData.xlsx
- SupplementaryInformation.docx
- SupplementaryData1.zip
- SupplementaryMovie1.mp4